

1 Glacier loss and vegetation expansion alter organic and inorganic carbon dynamics in high-
2 mountain streams

3
4 Andrew L. Robison¹, Nicola Deluigi¹, Camille Rolland¹, Nicola Manetti¹, and Tom Battin¹

5
6 ¹River Ecosystems Laboratory, Center for Alpine and Polar Environmental Research
7 (ALPOLE), Ecole Polytechnique Fédérale de Lausanne (EPFL), Lausanne, Switzerland.

8
9 Corresponding author: Andrew L. Robison, andrew.robison@epfl.ch

10 11 **Abstract**

12 High-mountain ecosystems are experiencing acute effects of climate change, most visibly
13 through glacier recession and the greening of the terrestrial environment. The streams
14 draining these landscapes are affected by these shifts, integrating hydrologic, geologic, and
15 biological signals across the catchment. We examined the organic and inorganic carbon
16 dynamics of streams in four Alpine catchments in Switzerland to assess how glacier loss and
17 vegetation expansion are affecting the carbon cycle of these high-mountain ecosystems. We
18 find that organic carbon concentration and fluorescence properties associated with humic-like
19 compounds increase with vegetation cover within a catchment, demonstrating the increasing
20 importance of allochthonous dissolved organic carbon sources following glacier retreat.
21 Meanwhile, streams transitioned from carbon dioxide sinks to sources with decreasing glacier
22 coverage and increased vegetation coverage, with chemical weathering and soil respiration
23 likely determining the balance. Periods of sink behavior were also observed in non-glaciated
24 streams, possibly indicating that chemical consumption of carbon dioxide could be more
25 common in high-mountain, minimally vegetated catchments than previously known.
26 Together, these results demonstrate the dramatic shifts in carbon dynamics of high-mountain
27 streams following glacier recession, with significant changes to both the organic and
28 inorganic carbon cycles. The clear link between the terrestrial and aquatic zones further
29 emphasizes the coupled dynamics with which all hydrologic and biogeochemical changes in
30 these ecosystems should be considered, including the carbon sink or source potential of
31 montane ecosystems.

32 33 **Short summary**

34 Climate change is affecting mountain ecosystems intensely, including the loss of glaciers and
35 the uphill migration of plants. How these changes will affect the streams draining these
36 landscapes is unclear. We sampled streams across a gradient of glacier and vegetation cover
37 in Switzerland and found glacier loss reduced the carbon dioxide sink from weathering, while
38 vegetation cover increased dissolved organic carbon in the stream. These changes are
39 important to consider for mountains globally.

40 41 **Keywords**

42 Streams, climate change, glaciers, carbon dioxide, organic carbon

43 1. Introduction

44 The effects of climate change on high-mountain areas are dramatic, with temperatures
45 increasing approximately twice as quickly as in lower elevation areas (IPCC, 2021). With
46 glacial retreat, the streams draining these landscapes are experiencing significant change in
47 the timing, magnitude, and source of flows (Kneib et al., 2020; Mackay et al., 2019). The
48 terrestrial environment is also shifting with the expansion of vegetation spatially (i.e., to
49 higher elevations) and temporally (i.e., longer growing season), which thereby impact the
50 hydrology, biogeochemistry, and ecology of catchment streams (Knight and Harrison, 2014;
51 Brighenti et al., 2019). In the Swiss Alps, recent work has highlighted the rapid “greening” of
52 high-mountain areas and decreasing snow and ice cover (Rumpf et al., 2022). While the
53 implications of climate change for terrestrial ecosystems have been examined broadly
54 (Finstad et al., 2016), the impact these changes will exert on the streams draining these
55 landscapes is much less explored (Beniston et al., 2018). Given the global extent and integral
56 role of streams in connecting high-mountain areas with downstream ecosystems (Milner et al.,
57 2017), exploring how these landscape alterations will affect the carbon dynamics of streams is
58 critical to contextualize their role in the global cycle (Horgby et al., 2019c).

59 High-mountain streams are tightly linked to the catchment they drain (Milner et al.,
60 2009; Brighenti et al., 2019). In particular, the presence of glaciers dominates stream
61 hydrology (Kneib et al., 2020), with significant biogeochemical and ecological implications.
62 For example, as glaciers generally provide the majority of water to their proglacial streams,
63 solute concentration and flux are frequently controlled by the contents and magnitude of
64 glacier melt water (Bergstrom et al., 2021). For example, dissolved organic carbon (DOC)
65 ice-locked within glaciers can be the dominant source of DOC to the proglacial stream upon
66 melting (Colombo et al., 2019). The lability of this glacier-derived DOC is often high, serving
67 as a major source of carbon fueling downstream metabolism (Hood et al., 2009). Glaciers are
68 also associated with high rates of geochemical weathering, both underneath the glacier
69 (Anderson et al., 1997) and in the proglacial stream (St. Pierre et al., 2019). The weathering of
70 both carbonate and silicate minerals can consume atmospheric carbon dioxide (CO₂), whereby
71 CO₂ dissolved in water is converted to bicarbonate through these reactions (Donnini et al.,
72 2016). These reactions involve significant transformations of dissolved inorganic carbon
73 (DIC) and potentially consume large amounts of CO₂ in the process (Hodson et al., 2000).

74 As glaciers shrink, there is generally a concomitant increase in soil development and
75 vegetation cover within catchments (Guelland et al., 2013). Higher vegetation cover and soil
76 development provides a pool of organic carbon for export to the streams (Garcia et al., 2015).
77 From this change, increases in stream DOC concentration are likely. Indeed, increased DOC
78 in aquatic ecosystems globally has been directly linked to the greening of the terrestrial
79 landscape (Finstad et al., 2016). Elevated aquatic DOC has implications for ecosystem
80 respiration, productivity, and water quality (Roulet and Moore, 2006; Hongve et al., 2004).
81 This change in DOC source also implies changes to the quality of stream organic matter
82 (Zhou et al., 2019), which could further alter stream metabolic regimes by promoting
83 heterotrophy (Bernhardt et al., 2017; Duarte and Prairie, 2005; Boix Canadell et al., 2020). In
84 terms of inorganic carbon, soils frequently represent the dominant source of CO₂ to streams,
85 as the products of soil respiration are transported to the stream via groundwater (Hotchkiss et
86 al., 2015). Thus, as soils develop and allow for the expansion of vegetation in mountain
87 catchments, emissions of CO₂ from the aquatic system may be promoted as the products of
88 soil respiration are transported to the stream and emitted.

89 Given these complex relationships, consideration of both glacial influence and the
90 terrestrial environment at-large is key to fully contextualize how climate change may alter
91 carbon flows to and from mountain streams. Moreover, both the organic and inorganic carbon
92 components must be evaluated to complete this cycle, providing perspective on the relative

93 influence of different catchment properties. In this study, we aim to evaluate landscape effects
94 on dissolved organic and inorganic carbon dynamics in high-mountain streams across a
95 glacial, vegetation, and elevation gradient. By comparing dissolved carbon concentration and
96 fluxes across these gradients, we can directly assess the relative impact of glacial retreat and
97 catchment greening. We hypothesized the presence of glaciers would drive CO₂ consumption
98 (St. Pierre et al., 2019), and the loss of glacier influence would elevate the role of catchment
99 soils as a source of CO₂ (Crawford et al., 2015). We also expected these landscape
100 transformations would increase the role of allochthonous dissolved organic carbon in the
101 stream (Fasching et al., 2016), with consequential changes to the quality of organic matter.
102

103 2. Methods

104 Samples of DOC and DIC were collected, as well as *in situ* sensor measurements of
105 dissolved carbon dioxide ($p\text{CO}_2$) in 12 streams in the high-mountain area of the western Swiss
106 Alps over five years, from 2016 to 2020. The sampling locations covered a broad range of
107 catchment glacier coverage, vegetation coverage, and elevation, providing for a space-for-
108 time substitution approach in which streams draining lower elevation, lower glacier cover,
109 and higher vegetation cover catchments represent potential future conditions of higher
110 elevation, higher glacier cover, and lower vegetation cover catchments. With this spatial
111 design, we can to evaluate how these carbon constituents may evolve with ecosystem
112 processes following anthropogenic climate change. Consideration of various other water
113 quality and catchment properties (e.g., dissolved oxygen, inorganic carbon isotopes, dissolved
114 organic matter fluorescence) provides further insight on changes in the relative contribution of
115 geochemical weathering, in-stream processes, and terrestrial inputs within these streams.
116

117 2.1 Site description

118 Our 12 stream sampling locations were equally distributed within Vallon de Nant,
119 Champéry, Valsorey and Val Ferret, four catchments in the western Swiss Alps (Figure 1).
120 These sites are part of the METALP project (<https://metalp.epfl.ch>), which has been described
121 extensively in previous studies (Ulseth et al., 2019; Boix Canadell et al., 2019; Horgby et al.,
122 2019c) and where numerous hydrological and biogeochemical parameters have been
123 monitored since 2016. The drainage areas vary from 0.31 km² to 23.2 km², and mean
124 catchment elevation from 1778 m to 2892 m (Table 1). Vegetation cover is highest at lower
125 elevations, and ranged from approximately 94% to 21% coverage of the catchment.
126

127
128 Figure 1: Map of the 12 study sites within four catchments of the Alps in southwestern
129 Switzerland (glacial cover and stream network from swissTLM3D; swisstopo).
130

131 The geology of the Champéry and Vallon de Nant catchments is dominated by the
132 presence of limestones, calcareous shales, and flysch (Burri et al., 1999). Val Ferret is
133 characterized by limestones and sandstones showing pronounced schistosity, while Valsorey
134 is underlain primarily by a metamorphic lithology that distinguishes with gneisses, crystalline
135 shales, and blue-grey schists. Additionally, in Valsorey, glacial cover accounts for about one
136 third of the total surface, with the blue-grey schists most prominent at high elevations beneath
137 and near the glaciers. Soils in this region are generally young, poorly developed leptosols and
138 fluvisols (Egli et al., 2010), with organic content that increases at lower elevations (Hoffmann
139 et al., 2014). While soil organic content has not been measured in these catchments,
140 measurements in nearby areas of the Swiss Alps have observed soil organic content ranging
141 from < 0.1 kg C m⁻² in soils around 2150 m elevation to around 2.0 kg C m⁻² at 1000 m
142 elevation (Hoffmann et al., 2014; Egli et al., 2010).

143 Table 1: Catchment characteristics.

144

145 2.2 *Grab sampling and sensor measurements*

146 Grab sampling of various physical and chemical parameters were made at all sampling
147 sites at approximately monthly intervals during the snow-free season. These parameters
148 include DOC, dissolved organic matter (DOM) fluorescence, major ions, $p\text{CO}_2$, DIC, and
149 alkalinity. The analysis of these analytes has been described previously (Horgby et al., 2019b;
150 Boix Canadell et al., 2019). Concentrations of major anions (Ca^{2+} , Mg^{2+} , K^+ , and Na^+) and
151 cations (SO_4^{2-} , NO_3^- , and Cl^-) were measured on streamwater filtered through 0.22- μm filters
152 (Mixed Cellulose Ester) using ion chromatography (Metrohm 930 Compact IC Flex; Aargau,
153 Switzerland).

154 Samples for the quantification of DOC and DOM fluorescence are filtered through
155 pre-combusted 0.45 μm GF/F filters (Whatman) into acid-washed and pre-combusted 40 mL
156 amber glass vials. Samples are kept refrigerated and analyzed for concentration within 24 h
157 from collection. DOC concentration was measured using a Sievers M5310C TOC Analyzer
158 (GE Analytical Instruments, New York, USA) with an accuracy of $\pm 2\%$ $\mu\text{g C L}^{-1}$, a precision
159 of $< 1\%$ relative standard deviation, and a detection limit of 22 $\mu\text{g C L}^{-1}$. Samples were taken
160 in triplicates and the mean concentration was used, with outliers removed if the concentration
161 exceeds three standard deviations from the mean. Calibration standards ranged from 0.05 to 1
162 mg C L^{-1} . DOM fluorescence excitation-emission matrices (EEMs) were created by
163 measuring fluorescence intensity of samples within a 1 cm cuvette across a range of excitation
164 (240–450 nm, 2 nm increment) and emission (211.19–620.23 nm, 2 nm increments)
165 wavelengths using an Aqualog® optical spectrometer (Horiba, Kyoto, Japan). Validation
166 scans are performed prior to sample analysis to validate instrument performance, such as
167 measuring the water Raman signal-to-noise ratio and emission calibration using a sealed,
168 standard cuvette of Milli-Q water (Type 1 LRW) to ensure the Raman peak position is at 297
169 $\text{nm} \pm 1 \text{ nm}$. Milli-Q water was used as a blank, which was used to remove background
170 fluorescence from the spectra. Absorbance was also measured within a 10 cm cuvette with a
171 Perkin Elmer Lambda 850 spectrophotometer (Massachusetts, USA).

172 Duplicate samples for dissolved inorganic carbon (DIC) concentration and the relative
173 stable carbon isotopic composition ($\delta^{13}\text{C}$ -DIC) were filtered through 0.2 μm membrane filters
174 into acid-washed 12 mL glass exetainer vials and stored refrigerated until analysis. Two mL
175 of sample were injected into synthetic air-filled, septum capped 12 mL exetainer vials
176 containing 200 μL 85% phosphoric acid to convert all DIC to gaseous CO_2 . The resulting gas
177 phase was then analyzed on the CRDS-SSIM2 equipped with a Small Sample Isotope Module
178 2 (CRDS-SSIM2, Picarro Inc., California, USA) and converted into DIC concentration.

179 Additionally, each monitoring station was instrumented with sensors measuring
180 physical and chemical parameters of the water or air at a 10 min frequency, including water
181 temperature, dissolved oxygen, carbon dioxide ($p\text{CO}_2$), and depth. Specifications, calibration
182 and maintenance procedures of these sensors have been described previously (Horgby et al.,
183 2019c; Boix Canadell et al., 2020). Stream $p\text{CO}_2$ was measured using a CARBOCAP®
184 GMP252 probe (Vaisala, Vantaa, Finland) within a porous polytetrafluoroethylene (ePDFE)
185 semi-permeable membrane. The probes were then protected with a fine-grained mesh, and a
186 metal casing. Raw data were adjusted according to the manufacturer's recommendations for
187 barometric pressure and water temperature. All $p\text{CO}_2$ sensors were tested in the laboratory
188 using certified gas mixtures of CO_2 diluted in synthetic air to final concentrations of 0, 400
189 and 2000 ppmv prior to deployment.

190 Discharge was calculated using rating curves relating water depth to discharge (Boix
191 Canadell et al., 2021), where direct measurements of discharge were made using slug
192 injections of sodium chloride (NaCl) as a conservative tracer (Gordon et al., 2004).

193 Additionally, when stream conditions allowed, 10 random measurements of stream depth
 194 were collected to provide a measure of average stream morphology to compare with
 195 measurements recorded by the sensor installed on the streamside.

196

197 2.3 CO₂ saturation and efflux

198 From the 10-minute sensor data, the daily median concentration of CO₂ was found for
 199 all sample locations during the monitoring period (Horgby et al., 2019c). The saturation and
 200 efflux for these values were then estimated using measurements of stream water temperature,
 201 and estimates of barometric pressure, atmospheric concentration of CO₂, and gas exchange
 202 velocity. Barometric pressure was obtained from the MeteoSwiss weather station network
 203 (Swiss Federal Office and Meteorology and Climatology). The Col du Grand St Bernard
 204 station (elevation 2473 m a.s.l.) was used for the Valsorey and Val Ferret catchments, while
 205 the Evionnaz station (482 m a.s.l.) and Les Diablerets (2964 m a.s.l.) stations were used for
 206 Champéry and Vallon de Nant stations. Barometric pressure at each monitoring stations (P_{site} ,
 207 mbar) was adjusted for site-specific elevation and temperature following:

208

$$209 \quad P_{\text{site}} = P_0 \exp\left(\frac{-gM(h-h_0)}{RT}\right), \quad (1)$$

210

211 where P_0 (mbar) is the barometric pressure measured at the MeteoSwiss station, h_0 and h (m)
 212 are the altitude of the meteorological and at the monitoring stations, respectively, g is the
 213 gravity acceleration (9.81 m s^{-2}), M the molar mass of air ($0.0289644 \text{ kg mol}^{-1}$) and R the
 214 universal gas constant ($8.31432 \text{ J mol}^{-1} \text{ K}^{-1}$). The temperature of air T_{air} ($^{\circ}\text{C}$) at the METALP
 215 stations is estimated through the temperature T_0 ($^{\circ}\text{C}$) measured at the MeteoSwiss station,
 216 where the regional temperature gradient $\Delta T/\Delta h$ is set to $-0.54 \text{ }^{\circ}\text{C}/100 \text{ m}$, obtained from air
 217 temperature data collected during the period 1990-2020 by the Evolène-Villa (1427 m a.s.l.)
 218 and the Montana (1825 m a.s.l.) weather stations (MeteoSwiss; Deluigi et al., 2017),

219

$$220 \quad T_{\text{air}} = T_0 - \left((h - h_0) \cdot \frac{\Delta T}{\Delta h}\right). \quad (2)$$

221

222 Sensor measurements of $p\text{CO}_{2,\text{raw}}$ (ppm) were then adjusted to site-specific
 223 temperature and barometric pressure following the ideal gas law:

224

$$225 \quad p\text{CO}_{2,\text{corr}} = p\text{CO}_{2,\text{raw}} \cdot \frac{P_{\text{site}}}{1013} \cdot \frac{298}{T_{\text{water}}}, \quad (3)$$

226

227 where P_{site} (mbar) is the barometric pressure at each location and T_{water} (K) is the measured
 228 water temperature. Dissolved CO₂ concentration ($\text{CO}_{2,\text{water}}$, $\mu\text{mol L}^{-1}$) was then derived by
 229 multiplying the corrected $p\text{CO}_{2,\text{corr}}$ with Henry's constant K_{H} ($\text{mol L}^{-1} \text{ atm}^{-1}$) at each site,

230

$$231 \quad \text{CO}_{2,\text{water}} = p\text{CO}_{2,\text{corr}} \cdot K_{\text{H}}. \quad (4)$$

232

233 K_{H} is a function of the water temperature in Kelvins (T_{water}) with A is 108.3865, B is
 234 0.01985076, C is -6919.53, D is -40.4515, E is 669365 according to Plummer and Busenberg
 235 (1982),

236

$$237 \quad K_{\text{H}} = 10^{A+B \cdot T_{\text{water}} + \frac{C}{T_{\text{water}}} + D \cdot \log_{10}(T_{\text{water}}) + \frac{E}{T_{\text{water}}^2}}. \quad (5)$$

238

239 A corresponding dissolved equilibrium concentration of CO₂ (CO_{2,sat}, μmol L⁻¹) was
 240 calculated for each sensor measurements at each site using an estimate of daily mean
 241 atmospheric CO₂ (CO_{2,air}),

$$242 \quad \text{CO}_{2,\text{sat}} = \text{CO}_{2,\text{air}} \cdot K_{\text{H}}, \quad (6)$$

243
 244 by adjusting measurements of CO₂ concentration at Jungfraujoch (freely available at
 245 <http://www.climate.unibe.ch>) for differences in barometric pressure and temperature,
 246

$$247 \quad \text{CO}_{2,\text{air}} = \text{CO}_{2,\text{Jungfrau}} \cdot \frac{P_{\text{site}}}{P_{\text{Jungfraujoch}}} \cdot \frac{T_{\text{Jungfraujoch}}}{T_{\text{site}}}. \quad (7)$$

248
 249 The standard gas transfer velocity (k₆₀₀, m d⁻¹) was calculated using the relationships
 250 developed by Ulseth et al. (2019) and extrapolated from the same 12 streams in this study:
 251

$$252 \quad \ln(k_{600}) \text{ for } eD > 0.02 = 1.18 \cdot \ln(eD) + 6.63 \quad (8)$$

$$253 \quad \ln(k_{600}) \text{ for } eD < 0.02 = 0.35 \cdot \ln(eD) + 3.10 \quad (9)$$

254
 255 where eD is the stream energy dissipation rate (m² s⁻³), which is obtained by multiplying the
 256 gravity acceleration (9.81 m s⁻²) with slope (S, unitless) and stream flow velocity (V, m s⁻¹),
 257

$$258 \quad eD = g \cdot S \cdot V \quad (10)$$

259
 260 Velocity was calculated according to the hydraulic geometry scaling proposed by (Horgby et
 261 al., 2019c) for these streams,
 262

$$263 \quad V = 0.668 \cdot Q^{0.365}, \quad (11)$$

264
 265 where Q is discharge (m³ s⁻¹). To convert k₆₀₀ to k_{CO₂} (Eq. 11) we used the temperature
 266 dependent Schmidt scaling according to (Wanninkhof, 2014),
 267

$$268 \quad Sc_{\text{CO}_2} = 1923.6 - 125.06 \cdot T_{\text{W}} + 4.3773 \cdot T_{\text{W}}^2 - 0.85681 \cdot T_{\text{W}}^3 + 0.00070284 \cdot T_{\text{W}}^4 \quad (12)$$

$$269 \quad k_{\text{CO}_2} = \frac{k_{600}}{\left(\frac{600}{Sc_{\text{CO}_2}}\right)^{-0.5}} \quad (13)$$

270
 271
 272 The CO₂ efflux (F_{CO₂}, g CO₂-C m⁻² d⁻¹) was then calculated as,
 273

$$274 \quad F_{\text{CO}_2} = k_{\text{CO}_2} \times (\text{CO}_{2,\text{water}} - \text{CO}_{2,\text{sat}}). \quad (14)$$

275
 276
 277
 278 *2.4 PARAFAC modelling*

279 Parallel factor analysis (PARAFAC) modelling of fluorescence excitation-emission
 280 matrices (EEMs) was used to identify and determine the main fluorescence components of
 281 DOM present across collected water samples and was conducted using the R packages
 282 *staRdom* (Pucher et al., 2019) and *eemR* (Massicotte, 2019). Pre-processing of EEMs was
 283 necessary prior to PARAFAC development (Murphy et al., 2013; Stedmon & Bro, 2008).
 284 Briefly, spectra were corrected for instrument-specific effects, blank subtraction, inner-filter
 285 effects. First- and second-order Rayleigh scattering was removed and corrected EEMs

286 normalized to Raman units (Murphy et al., 2010). A total of 220 samples were included for
287 model development. The final PARAFAC model was validated using split-half analysis. The
288 resulting components were compared to previously published fluorescence components from
289 aquatic ecosystems in the OpenFluor database (Murphy et al., 2014).

290

291 *2.5 Statistical analyses*

292 All statistical analyses were performed in MATLAB and Statistics Toolbox Release
293 2021a (MathWorks, Massachusetts, USA). Differences in concentration or saturation between
294 groups of streams was investigated using Kruskal-Wallis tests. Simple linear regression was
295 used to evaluate relationships between DOC concentration or CO₂ saturation with catchment
296 properties and water quality parameters. The Pearson correlation coefficient (r) and
297 coefficient of determination (r^2) were used to determine the strength of correlations, with the
298 Pearson correlation coefficient used to show the direction of interaction.

299 The highly correlated nature of potential explanatory variables limited interpretability
300 for CO₂ saturation, thus we used partial least squares (PLS) regression to identify variables
301 important for predicting median CO₂ saturation at each site. PLS is a method which is well-
302 designed for datasets with many collinear predictor variables and when the number of
303 observations is small relative to the number of predictor variables (Wold et al., 1984;
304 Carrascal et al., 2009; Nash and Chaloud, 2011). Here, our response variable is the median
305 CO₂ saturation of each stream location, and 39 predictor variables (standardized within the
306 PLS model) are included (Table S1).

307 A Monte-Carlo cross-validation method assessed the predictive ability of the resulting
308 PLS model, where the model was fitted with a sub-sample of data. The calibration validation
309 ratio was set to 0.8, following Onderka et al. (2012), then the resulting fitted models were
310 tested on the validation set. This process was repeated 500 times. The mean cross-validated
311 goodness of prediction (Q^2) was then compared to the original model fit (R^2Y). The strength
312 of each predictor variable within the model was then analyzed using variable importance in
313 the projection (VIP), where highly important variables had $VIP > 1.0$ (Eriksson et al., 2001).
314 Additionally, moderately important ($0.8 < VIP < 1.0$) or less influential ($VIP < 0.8$) variables
315 were identified.

316 Finally, catchment areal fluxes of CO₂, DIC, and DOC were calculated using
317 catchment area and estimates of stream surface area. We focus on the snow-free period, July 1
318 through October 31 (Deluigi et al., 2017), to exclude snow cover as a confounding factor
319 affecting gas exchange. Concentration and gas exchange rates are considered constant within
320 subcatchments. An estimation of the network stream area was computed as the product of the
321 stream length and width during this snow free period. Perennial stream length was extracted
322 from the large-scale topographic landscape model of Switzerland (swissTLM3D) and
323 compared to a 2m-resolution DEM stream network (swissALTI3D). Considering the
324 complexity of the network and its remoteness, stream widths were estimated on aerial images
325 with a 25 cm pixel resolution, with a minimum of one width measurement per stream order.
326 An average of 187 width estimates were made per catchment. The calculation of areal flux for
327 CO₂ is particularly uncertain as stream surface area (Paillex et al., 2020), gas exchange
328 (Ulseth et al., 2019), and $p\text{CO}_2$ (Horgby et al., 2019b) are each highly dynamic in high-
329 mountain river networks. Thus, these estimates remain approximations intended to provide
330 perspective on the relative balance of dissolved carbon constituents in these stream networks
331 rather than robust calculations of flux. We consider CO₂ as a vertical flux, either into or out of
332 the stream, while DOC and DIC are downstream fluxes. The downstream DIC flux inherently
333 includes downstream transport of CO₂.

334

335 **3. Results**

336 *3.1 Dissolved carbon concentrations*

337 The overall median concentration of DOC was 0.22 mg C L⁻¹, with site specific
338 median concentrations ranging from 0.12 mg C L⁻¹ at the upper Val Ferret site (FEU), to 0.45
339 mg C L⁻¹ in the tributary stream at Vallon de Nant (RIC) (Figure 2a; Table 2). All measured
340 DOC concentrations (212 samples) were below 1.00 mg C L⁻¹. From simple linear regression,
341 median DOC concentration at a site varied most strongly with catchment vegetation cover (r =
342 0.76), δ¹³C-DIC values (r = -0.75), and catchment glacier cover (r = -0.53).

343
344 Table 2: Median concentration of DOC and DIC, percent saturation of CO₂ and O₂, and
345 isotopic composition of DIC for the 12 sites. Concentration and isotopic composition are
346 summarized from grab samples, while CO₂ and O₂ saturation are summarized from sensor
347 data.

348
349 Figure 2: Boxplots of a) DOC and b) DIC concentration (mg L⁻¹) from grab samples, and c)
350 CO₂ saturation (%) derived from sensor measurements.

351
352 Concentrations of DIC were generally greater and more varied than DOC, with an
353 overall median DIC concentration of 1.77 mg C L⁻¹ across 191 samples, ranging between 0.79
354 and 2.65 mg C L⁻¹ (Figure 2b). DIC concentration was most strongly correlated to decreasing
355 mean catchment elevation (r = -0.67), with the three relatively high elevation Valsorey
356 locations exhibiting significantly lower median concentrations than the other nine sites (p <
357 0.01). The median δ¹³C-DIC value across sites was -6.14‰ (Table 2). The Champéry
358 locations exhibited the most depleted δ¹³C-DIC values (median = -9.28‰), which were
359 significantly lower than the remaining nine streams (p = 0.02).

360 Across all streams, the median saturation of CO₂ was 95.1%, with the lowest median
361 saturation of 68.1% measured at the upstream location at Valsorey (VAU) and the highest
362 median saturation of 137% measured at the upstream location at Val Ferret (FEU; Figure 2c).
363 All sites exhibited periods of oversaturation and undersaturation, except for VAU, where
364 undersaturation was always observed. CO₂ saturation was significantly positively correlated
365 with specific conductivity, alkalinity, DIC, and calcium, and negatively correlated with
366 glacier coverage and specific UV absorbance at 254 nm (SUVA₂₅₄). However, the variance
367 explained by any of these individual variables was low (r² < 0.3). A three-component PLS
368 model was extracted which explained roughly 49% of the variance in median CO₂ saturation
369 (R²Y = 0.49), with moderate predictive power (Q² = 0.42). Ten variables were deemed highly
370 influential (VIP > 1). These include catchment characteristics of mean catchment elevation,
371 catchment area, glacier cover, and vegetation cover. Additionally, water quality parameters
372 deemed influential were specific conductivity, sulfate and calcium concentration, total
373 suspended solids, and discharge. Additionally, DOC was identified as a moderately influential
374 variable.

375 Dissolved oxygen saturation was much less variable than CO₂ across sites, with
376 median values between 98% and 100% and periods of over- and undersaturation for all sites
377 (Table 2). Similarly, the interquartile range of CO₂ saturation across all sites was large,
378 38.1%, when compared to that of dissolved oxygen, 2.3%. The major cation across sites was
379 Ca²⁺, and the major anion was SO₄²⁻ (Table S2). The log ratios of Mg²⁺ and Ca²⁺ to SO₄²⁻ are
380 similar across sites (Figure 3), clustering closest to carbonate end-members (Torres et al.,
381 2017). Within larger catchments, only the tributary site within the Val Ferret catchment (PEU)
382 differs significantly from the main stem stream locations.

383
384 Figure 3: Stoichiometry of dissolved ion in the twelve study streams and from a global
385 database of 95 glacier-fed streams (Torres et al., 2017). The range of each lithological end-

386 member are shown by the boxes. The tributary stream in the Val Ferret catchment (PEU) is
387 shown as it is clearly distinguished from the main stream locations.

388

389 3.2 PARAFAC modelling results

390 PARAFAC modelling resulted in a four-component model (Figure S1). In comparing
391 these components to the OpenFluor database, the first (C1) and second component (C2) are
392 likely of terrestrial humic origin, while the third (C3) and fourth (C4) are proteinaceous, likely
393 of microbial origin (Kida et al., 2019). The components resemble those reported from other
394 freshwater and glacial environments (e.g., Spencer et al. 2014, Imbeau and Vincent 2021,
395 Kida et al. 2021). When compared to EEM fluorophore peaks assigned by Coble et al. (1990,
396 1998), C1 appears to reflect the A and C peaks which are associated with humic-like
397 compounds from biodegradation of terrestrial plant matter, while C2 contains peak M, which
398 is linked to humic-like compounds related to primary production. Similarly, C3 appears like
399 the T peak and C4 the B peak, both of which are suggested to be proteinaceous compounds of
400 microbial origin. In general, the humic-associated components were found in greater intensity
401 (median = 0.038 and 0.024 RU for C1 and C2, respectively) than the protein-associated
402 components (median = 0.019 and 0.008 RU for C3 and C4, respectively). Both of the humic-
403 associated components were significantly positively correlated with DOC concentration
404 across all sites, C1 ($r = 0.86$) and C2 ($r = 0.69$) (Figure 4). The protein-associated peaks
405 showed little correlation with DOC concentration ($r^2 \leq 0.2$).

406

407 Figure 4: Intensity of the four components within the PARAFAC model against DOC
408 concentration from grab samples, with catchment vegetation cover shown by color. a)
409 Component 1 and b) component 2 represent humic-like compounds while c) component 3 and
410 d) component 4 represent proteinaceous compounds. The coefficient of determination (r^2) is
411 shown for each linear regression.

412

413 3.3 Catchment carbon fluxes

414 Total areal fluxes of dissolved carbon during the snow-free period ranged from -0.027
415 to 0.052 g C m⁻² catchment area d⁻¹, at the upstream Valsorey and downstream Champéry
416 locations, respectively (Figure 5). Considering absolute fluxes, the vertical flux of CO₂ was
417 the largest component of the dissolved carbon flux, contributing a median of 67%. The
418 downstream flux of DIC (which includes dissolved CO₂) contributed 29% to the total carbon
419 flux, and DOC contributed the least (4%). Negative net fluxes of C represent occasions when
420 the stream is estimated to be a net sink of CO₂, and this sink exceeds the downstream
421 transport of DOC and DIC. This occurred in only a single catchment (Valsorey).

422

423 Figure 5: Estimated annual fluxes of the dissolved carbon components (CO₂, DOC, and DIC)
424 normalized for catchment area. DOC and DIC are downstream fluxes, while CO₂ is a vertical
425 flux. The DIC flux includes downstream transport of CO₂.

426

427 4. Discussion

428 Comparing the dissolved carbon constituents in stream water within the space-for-time
429 framework provided by these 12 study sites highlights how the changing nature of high-
430 mountain catchments will have dramatic effects on the stream carbon cycle. There is a clear
431 difference in DOC between higher and lower elevation sites, likely as allochthonous carbon
432 becomes more important with increasing vegetation cover at lower elevation. The saturation
433 of CO₂ appears related to these DOC inputs, not only as a potential source of carbon for in-
434 stream respiration, but also as an indicator of an increasing importance of soil-derived CO₂ to
435 the stream. Geochemical weathering remains a significant sink of CO₂, most strongly in

436 glaciated catchments. However, the relevance of geochemical weathering to the CO₂ budget is
437 not limited to glaciated catchments, as periods of under-saturation were observed in non-
438 glaciated streams. The dissolved carbon dynamics of montane streams are thus critically tied
439 to the dissolved carbon dynamics of high-mountain streams.

440

441 *4.1 Increasing allochthonous DOC in high-mountain streams*

442 The observed relationships between DOC concentration and catchment vegetation
443 cover, and even more strongly the humic-like components of the DOM pool, suggest
444 allochthonous sources drive the increase in DOC concentration across these high-mountain
445 streams. Higher stream DOC concentration has been attributed to greater terrestrial inputs and
446 increasing vegetation cover (Zhou et al., 2019; Pain et al., 2020), as well as decreasing glacier
447 influence (Fellman et al., 2010). The routing of water through catchment soils should thus
448 play an increasingly large role in determining the timing and magnitude of allochthonous
449 carbon export to high-mountain streams generally. For example, as the terrestrial environment
450 becomes a more important source of DOC to streams, so too should hydrologic transport
451 (Gómez-Gener et al., 2021). For example, in our study streams, DOC export has been shown
452 to be strongly related to discharge patterns, with snowmelt mobilizing additional DOC
453 compared to other seasons (Boix Canadell et al., 2019; Boyer et al., 1997). Similarly, rain
454 events should then be related to increased humic-like DOM inputs from terrestrial sources as
455 transport from hillslope to stream is amplified (Fasching et al., 2016). While the indication of
456 allochthony from DOM optical properties is imperfect (Begum et al., 2023; Guillemette and
457 del Giorgio, 2012), the complementary DOC concentration patterns with vegetation cover and
458 elevation reinforce the interpretation of these data.

459 Vegetation cover, as used in this study, serves as a broad indicator of soil development
460 within these catchments, where accumulation of soil material allows for vegetation expansion
461 (Hagedorn et al., 2019; Henne et al., 2011). The use of vegetation cover as a proxy for soil
462 development following deglaciation is accurate in early successional stages (Klaar et al.,
463 2014), which is true of the catchments in this studies. The development of soil, as indicated by
464 increasing vegetation cover, can increase the pool of organic carbon in glacier forelands
465 (Wietrzyk-Pelka et al., 2020; Dümig et al., 2011; Egli et al., 2010), which can then be a
466 source or organic carbon to the proglacial stream (Zah and Uehlinger, 2001). For example, in
467 glacier fed streams in Canada, stream DOC concentration increased with catchment soil
468 development (slope $\approx 0.2 \text{ mg C L}^{-1} \text{ soil \% catchment area}^{-1}$; Lafrenière and Sharp, 2004),
469 similar to our relationship with vegetation (slope = $0.05 \text{ mg C L}^{-1} \text{ vegetation \% catchment}$
470 area^{-1}). Either of these metrics, vegetation or soil, are indicative of significant catchment
471 change with implications for terrestrial-aquatic carbon transfers.

472 Considering the greening of the terrestrial environment in the Alps (Rumpf et al.,
473 2022), it follows that the streams draining these landscapes may be expected to experience an
474 increase in DOC concentration of terrestrial origin. Our results support this hypothesis, in
475 which stream DOC concentration and the humic-like components likely of allochthonous
476 origin increase with catchment vegetation cover. These changes have potentially important
477 implications for these streams as well as their downstream ecosystems, from altering
478 metabolic regimes by promoting heterotrophy (Hall et al., 2016), limiting primary
479 productivity (Kritzberg et al., 2019), and causing higher drinking water production costs
480 (Hongve et al., 2004). Even while relatively low in concentration, the foundational physical,
481 biochemical, and ecological nature of DOC within streams magnifies the impact of these
482 changes in DOC concentration and highlight the substantial consequences of vegetation
483 expansion following glacial retreat.

484

485 *4.2 Terrestrial biogeochemical processes drive aquatic CO₂ saturation patterns*

486 With regards to CO₂, extensive periods of undersaturation are relatively rare in
487 riverine systems, but are likely explained by geochemical weathering (St. Pierre et al., 2019).
488 In our study, the isotopic signature of DIC provides the primary evidence of geochemical
489 weathering, where depleted $\delta^{13}\text{C}$ -DIC values (approximately -9 to -3‰) relative to
490 atmospheric equilibrium are indicative of weathering (Skidmore et al., 2004). This agrees well
491 with glacier-fed streams in Alaska (-7 to 0‰; St. Pierre et al. 2019), and mineral sources of
492 DIC have been highlighted in Swiss high-mountain streams previously (Horgby et al., 2019c).
493 Furthermore, the PLS model results also distinguish influential factors related to the products
494 of weathering (i.e., specific conductivity, sulfate and calcium concentration) or which affect
495 the rate of weathering (i.e., glacier cover, runoff, total suspended solids). As such, the role of
496 weathering in consuming CO₂ appears substantial.

497 The importance of geochemical weathering as a CO₂ sink in high-mountain areas is
498 well described (Hilton and West, 2020; Donnini et al., 2016), where rapid weathering of
499 carbonate and silicate rock consumes CO₂. In particular, elevated rates of weathering are
500 expected for subglacial environments, where water flows over recently crushed, fine-grained
501 reactive mineral surfaces (Tranter, 2003; Sharp et al., 1995). This process can continue in
502 proglacial streams, where suspended sediments with high surface areas promote continued
503 CO₂ drawdown (St. Pierre et al., 2019). Indeed, we see the lowest CO₂ saturation at the two
504 most glacially influenced streams (VAU and VAD) within the Valsorey catchment. Glacially
505 enhanced weathering thus appears significant in this study as well.

506 Still, with periods of CO₂ undersaturation in all our study catchments, geochemical
507 weathering appears to be relevant regardless of the presence of the glacier. To further
508 constrain weathering as the primary sink of CO₂ in these catchments, we can also assess the
509 potential for carbon fixation via photosynthesis as an alternative cause of undersaturation.
510 With oxygen saturation consistently near or below saturation in all streams, photosynthesis is
511 an unlikely driver of CO₂ undersaturation, as oxygen must inherently be above saturation to
512 balance carbon fixation. Productivity has been shown to be limited in these streams outside of
513 small temporal windows of opportunity (Boix Canadell et al., 2021), further reducing the
514 likelihood. Lastly, the lack of variability in oxygen saturation across streams suggests
515 photosynthetic rates do not vary significantly across streams, thus cannot account for the
516 observed variability in CO₂ saturation.

517 In contrast, variability within the DIC isotopic data does help explain the contribution
518 of CO₂ to streams derived from the oxidation of organic matter in the terrestrial environment.
519 The effect of organic carbon oxidation on $\delta^{13}\text{C}$ -DIC values is depletion, i.e., more negative
520 values (Pawellek and Veizer, 1994). It is thus likely the depleted $\delta^{13}\text{C}$ -DIC values observed at
521 the Champéry streams are a result of greater rates of organic carbon oxidation, where the pool
522 of organic carbon is evinced by the high vegetation cover and stream DOC concentration. We
523 can more narrowly identify this process as most likely occurring in catchment soils, as the
524 near-equilibrium nature of oxygen and the relatively low concentrations of DOC suggests a
525 minor role for in-stream respiration (Bernhardt et al., 2017). Stream CO₂ is generally
526 supported by external sources of CO₂ such as soil respiration (Hotchkiss et al., 2015;
527 Campeau et al., 2019), and has been shown for mountain streams in particular (Clow et al.,
528 2021; Crawford et al., 2015). Thus, as soils develop and organic carbon accumulates, the
529 potential for terrestrially derived CO₂ inputs to the stream increases and CO₂ saturation
530 increases (Marx et al., 2017). The role of the terrestrial environment in affecting stream CO₂
531 saturation is reinforced by the PLS model, which selected both vegetation cover and DOC
532 concentration as influential variables. As such, there appears to be a link between increasing
533 CO₂ saturation in these streams and organic matter accumulation and processing in the
534 terrestrial environment.

535 Given the importance of geochemical weathering to the carbon dynamics of these
536 catchments, consideration of geological variability between sites is necessary. While major
537 lithologies are dissimilar across sites (Table 1), the ratios of major ions are remarkably similar
538 and highlight the importance of carbonate weathering across all sites (Figure 3). While
539 carbonate-containing lithologies are clear in three of the catchments (Vallon de Nant,
540 Champéry, Val Ferret), the carbonate-like signal in the Valsorey area is likely explained by
541 high levels of calcite in the blue-grey schists (Bucher et al., 2017). This schist is primarily
542 located beneath and near the glacier (Burri et al., 1999), thus glacier-enhanced weathering
543 may disproportionately affect the weathering of this mineral. The prominence of carbonate
544 weathering in these study streams may also indicate that the potential for geochemical
545 weathering to serve as a CO₂ sink is elevated compared to glacier-fed streams globally
546 (Torres et al., 2017). That is, catchments with lower proportions of carbonate-containing
547 lithologies likely have lower potential as geochemical CO₂ sinks (St. Pierre et al., 2019). This
548 elevated weathering as a result of carbonate-rich lithology is exemplified by the tributary
549 stream in the Val Ferret catchment (Figure 3). Despite no glacier coverage within this
550 subcatchment, the median CO₂ saturation is undersaturated (Table 2). This is likely explained
551 by the abundance of limestone deposits, which weather relatively quickly and geochemically
552 consume CO₂. In expanding these analyses of carbon to other regions and mountain ranges,
553 direct geologic perspectives will be needed to differentiate potential geochemical weathering
554 rates (Hilton and West, 2020), and hence the potential for CO₂ consumption.

555

556 *4.3 Conceptual model of carbon budgets in glacierized catchments*

557 Altogether, these results provide the basis of a simple conceptual model explaining
558 contributions to stream CO₂, thereby explaining saturation dynamics across glacier, soil, and
559 elevation gradients in mountain catchments (Figure 6). Across the entire range of elevation,
560 geochemical weathering acts as a sink of CO₂ (Crawford et al., 2019), where the intensity of
561 this sink is dependent in large part on catchment geology. Where present, glaciers can provide
562 additional weathering potential, whereby higher concentrations of suspended sediment
563 increase mineral surface area greatly (St. Pierre et al., 2019). Moreover, this elevated
564 weathering potential can extend far downstream depending on the suspension and transport of
565 glacial till. Decreasing glacier influence reduces total weathering potential, but CO₂
566 undersaturation as a result of weathering is not limited to glacierized catchments. With the
567 development of soils within the catchment, inputs of allochthonous organic carbon and CO₂
568 increases, elevating CO₂ concentrations. This CO₂ likely derives primarily from soil
569 respiration rather than in-stream respiration of organic carbon (Clow et al., 2021; Singer et al.,
570 2012).

571

572 Figure 6: Conceptual model of processes affecting CO₂ saturation, and thus direction of flux,
573 across glacier, soil, and elevation gradients within glacierized catchments. Geochemical
574 weathering is important across the entire landscape, but is enhanced under glaciated
575 conditions and nearness to the glacier. As vegetation and soil develop at lower elevation,
576 terrestrial inputs add CO₂ through direct inputs from soil respiration and from organic carbon
577 inputs which fuel in-stream respiration. The net balance of these processes determines the
578 CO₂ saturation. In the aerial image of the Valsorey catchment, the transition from glacier to
579 vegetation cover can be seen directly (from Google Earth 2023).

580

581 Estimated fluxes of dissolved carbon constituents further support this conceptual
582 model and the dominant role of terrestrial processes in determining the relative balance within
583 and between streams. First, the dominance of CO₂ to the absolute total flux emphasizes the
584 significance of gaseous carbon effluxes across within river networks. Our result of 67%

585 contribution from CO₂ is similar to a study of a boreal catchment in Sweden, in which CO₂
586 accounted for 53% of the net carbon flux (Wallin et al., 2013). Similarly, In a glaciated
587 catchment in Alaska (St. Pierre et al., 2019), the areal rate of CO₂ flux was found to be -0.38 g
588 C m⁻² catchment area d⁻¹, an order of magnitude higher than our most highly glaciated system
589 (-0.03 g C m⁻² catchment area d⁻¹ at VAU). Following our conceptual model, the difference is
590 explained by the much more heavily glaciated area of the Alaskan catchment (> 40%) and the
591 limitation of the sampling period to the most intense glacial melt period (June – August).
592 When glacier influence is highest, the potential for weathering is highest as well, driving
593 consumption of CO₂. Yet, even without glacier influence, consumption of CO₂ through
594 weathering is still possible within the catchment and should be considered in montane stream
595 carbon budgets.

596 DIC contributes 29% to the total carbon flux, DOC contributes the least, generally
597 indicating a greater influence of mineral processes rather than organic (Rehn et al., 2022). The
598 low contribution of DOC differs greatly from the Swedish boreal catchment, where DOC
599 contributed roughly 40% on average (Wallin et al., 2013). This difference not only highlights
600 the limited soil development within high-mountain systems, but also the potential for
601 increased DOC export to the stream with continued soil development. Nonetheless, as DOC
602 contribution clearly increased with additional vegetation cover across our study systems, the
603 role of the terrestrial landscape in supporting stream organic carbon content is clear.

604 Our focus on broad relationships across these 12 locations recognizably conceals how
605 local conditions and seasonality may affect site specific dynamics. Previous analyses have
606 examined CO₂ and DOC individually at these stream locations, and provide some perspective.
607 On a finer spatial scale within the stream network, local groundwater inputs can
608 disproportionately elevate CO₂ concentration (Horgby et al., 2019b), which could be a useful
609 tool in more directly quantifying terrestrial inputs to streams. Seasonally, the clearest pattern
610 of *p*CO₂ indicates elevated contributions of terrestrial CO₂ during the spring snowmelt
611 (Horgby et al., 2019a). Further differentiating temporal patterns during shorter timescales,
612 such as storm events, may be useful in elucidating the contribution of soil respiration to the
613 streams (Marzolf et al., 2022). While there is surely more to be learned at these finer spatial
614 and temporal scales of both organic and inorganic carbon, our focus on broad scale patterns
615 across catchments allows us to make more generalizable conclusions. Given the strength of
616 the observed relationships within our analyses and their consistency with other studies of
617 high-mountain streams, our conceptual model provides a simple, yet important foundation
618 with which to assess carbon dynamics in montane streams globally.

619

620 **5. Conclusion**

621 The organic and inorganic components of the dissolved carbon pool shift across a
622 glacier and vegetation gradient, driven by the relative balance of geochemical weathering and
623 terrestrial carbon inputs to the stream. Our results also highlight an expanded importance of
624 geochemical weathering in high-mountain ecosystems globally, whereby carbonate and
625 silicate weathering may consume CO₂ across more mountain landscapes than previously
626 considered (Horgby et al., 2019c). Implications for landscape carbon balances are clear, with
627 decreased potential for CO₂ uptake and increased emissions of terrestrially-derived CO₂
628 emerging after glacier retreat and landscape greening. The rate of the transition from carbon
629 sink to source is likely accelerated by climate change (Knight and Harrison, 2014), thus
630 continued examination of the contributions of these processes to net stream balances is critical
631 to predicting the future role of mountain catchments in the global carbon cycle.

632

633 **Data availability**

634 Data used in this analysis is available through the METALP data portal (<https://metalp->
635 [data.epfl.ch/](https://metalp-data.epfl.ch/)) or through publicly accessible university and government portals (e.g.,
636 <http://www.climate.unibe.ch> or <http://map.geo.admin.ch>).
637

638 **Author contributions**

639 TB secured funding for the research. ND and CR performed field and laboratory analyses.
640 AR, ND, CR, and NM processed and analyzed the results. AR conducted statistical analyses.
641 ND performed geospatial analyses. AR led manuscript development and revised the
642 manuscript with input from all co-authors.
643

644 **Competing interests**

645 The authors declare that they have no conflict of interest.
646

647 **Acknowledgements**

648 The research leading to these results has received funding from the Swiss Science Foundation
649 grant agreement 200021_163015 (METALP project). We thank Dr. Hannes Peter for assistance
650 in analyzing the fluorescent properties of dissolved organic matter and for providing feedback
651 in manuscript development. We also acknowledge members of the RIVER lab for assistance in
652 field work and laboratory analyses.

653 **References**

- 654 Anderson, S. P., Drever, J. I., and Humphrey, N. F.: Chemical weathering in glacial
655 environments, *Geology*, 25, 399–402, [https://doi.org/10.1130/0091-](https://doi.org/10.1130/0091-7613(1997)025<0399:CWIGE>2.3.CO)
656 [7613\(1997\)025<0399:CWIGE>2.3.CO](https://doi.org/10.1130/0091-7613(1997)025<0399:CWIGE>2.3.CO), 1997.
- 657 Begum, M. S., Park, J. H., Yang, L., Shin, K. H., and Hur, J.: Optical and molecular indices
658 of dissolved organic matter for estimating biodegradability and resulting carbon dioxide
659 production in inland waters: A review, *Water Res.*, 228, 119362,
660 <https://doi.org/10.1016/j.watres.2022.119362>, 2023.
- 661 Beniston, M., Farinotti, D., Stoffel, M., Andreassen, L. M., Coppola, E., Eckert, N., Fantini,
662 A., Giacona, F., Hauck, C., Huss, M., Huwald, H., Lehning, M., López-Moreno, J. I.,
663 Magnusson, J., Marty, C., Morán-Tejeda, E., Morin, S., Naaim, M., Provenzale, A., Rabatel,
664 A., Six, D., Stötter, J., Strasser, U., Terzago, S., and Vincent, C.: The European mountain
665 cryosphere: A review of its current state, trends, and future challenges, *Cryosphere*, 12, 759–
666 794, <https://doi.org/10.5194/tc-12-759-2018>, 2018.
- 667 Bergstrom, A., Koch, J. C., O’Nee, S., and Baker, E.: Seasonality of solute flux and water
668 source chemistry in a coastal glacierized watershed undergoing rapid change: Wolverine
669 Glacier watershed, Alaska, *Water Resour. Res.*, 57, e2020WR028725,
670 <https://doi.org/10.1029/2020WR028725>, 2021.
- 671 Bernhardt, E. S., Heffernan, J. B., Grimm, N. B., Stanley, E. H., Harvey, J. W., Arroita, M.,
672 Appling, A. P., Cohen, M. J., Mcdowell, W. H., Hall, R. O., Read, J. S., Roberts, B. J., Stets,
673 E. G., and Yackulic, C. B.: The metabolic regimes of flowing waters, *Limnol. Oceanogr.*,
674 63,S99–S118, <https://doi.org/10.1002/lno.10726>, 2018.
- 675 Boix Canadell, M., Escoffier, N., Ulseth, A. J., Lane, S. N., and Battin, T. J.: Alpine glacier
676 shrinkage drives shift in dissolved organic carbon export from quasi-chemostasis to transport
677 limitation, *Geophys. Res. Lett.*, 46, 8872–8881, <https://doi.org/10.1029/2019GL083424>,
678 2019.
- 679 Boix Canadell, M., Gómez-Gener, L., Cléménçon, M., Lane, S. N., and Battin, T. J.: Daily
680 entropy of dissolved oxygen reveals different energetic regimes and drivers among high-
681 mountain stream types, *Limnol. Oceanogr.*, 66, 1594–1610,
682 <https://doi.org/10.1002/lno.11670>, 2020.
- 683 Boix Canadell, M., Gómez-Gener, L., Ulseth, A. J., Cléménçon, M., Lane, S. N., and Battin,
684 T. J.: Regimes of primary production and their drivers in Alpine streams, *Freshw. Biol.*, 66,
685 1449–1463, <https://doi.org/10.1111/fwb.13730>, 2021.
- 686 Boyer, E. W., Hornberger, G. M., Bencala, K. E., and McKnight, D. M.: Response
687 characteristics of DOC flushing in an alpine catchment, *Hydrol. Process.*, 11, 1635–1647,
688 [https://doi.org/10.1002/\(SICI\)1099-1085\(19971015\)11:12<1635::AID-HYP494>3.0.CO;2-H](https://doi.org/10.1002/(SICI)1099-1085(19971015)11:12<1635::AID-HYP494>3.0.CO;2-H),
689 1997.
- 690 Brighenti, S., Tolotti, M., Bruno, M. C., Wharton, G., Pusch, M. T., and Bertoldi, W.:
691 Ecosystem shifts in Alpine streams under glacier retreat and rock glacier thaw: A review, *Sci.*
692 *Total Environ.*, 675, 542–559, <https://doi.org/10.1016/j.scitotenv.2019.04.221>, 2019.
- 693 Bucher, K., Zhou, W., and Strober, I.: Rocks control the chemical composition of surface
694 water from the high Alpine Zermatt area (Swiss Alps), *Swiss J. Geosci.*, 110, 811–831,
695 <https://doi.org/10.1007/s00015-017-0279-y>, 2017.
- 696 Burri, M., Allimann, M., Chessex, R., Piaz, G. V. D., Valle, G. Della, Bois, L. Du, Gouffon,

697 Y., Guermani, A., Hagen, T., Krummenacher, D., and Looser, M. . O.: Chanrion (CN 1346)
698 including Mont Vélan (CN 1366), in: Geological Atlas of Switzerland 1:25000. Bundesamt
699 für Landestopografie swisstopo, edited by: Burri, M., Piazz, G. V. D., Valle, G. Della,
700 Gouffon, Y., and Guermani, A., 1999.

701 Campeau, A., Bishop, K., Amvrosiadi, N., Billett, M. F., Garnett, M. H., Laudon, H., Öquist,
702 M. G., and Wallin, M. B.: Current forest carbon fixation fuels stream CO₂ emissions, *Nat.*
703 *Commun.*, 10, 1876, <https://doi.org/10.1038/s41467-019-09922-3>, 2019.

704 Carrascal, L. M., Galván, I., and Gordo, O.: Partial least squares regression as an alternative
705 to current regression methods used in ecology, *Oikos*, 118, 681–690,
706 <https://doi.org/10.1111/j.1600-0706.2008.16881.x>, 2009.

707 Clow, D. W., Striegl, R. G., and Dornblaser, M. M.: Spatiotemporal dynamics of CO₂ gas
708 exchange from headwater mountain streams, *J. Geophys. Res. Biogeosciences*, 126,
709 e2021JG006509, <https://doi.org/10.1029/2021JG006509>, 2021.

710 Coble, P. G., Greent, S. A., Blought, N. V, and Gagosiant, R. B.: Characterization of
711 dissolved organic matter in the Black Sea by fluorescence spectroscopy, *Nature*, 348, 432–
712 435, <https://doi.org/doi.org/10.1038/348432a0>, 1990.

713 Coble, P. G., Castillo, C. E. Del, and Avril, B.: Distribution and optical properties of CDOM
714 in the Arabian Sea during the 1995 Southwest Monsoon, *Deep Sea Res. Part II Top. Stud.*
715 *Oceanogr.*, 45, 2195–2223, [https://doi.org/10.1016/S0967-0645\(98\)00068-X](https://doi.org/10.1016/S0967-0645(98)00068-X), 1998.

716 Colombo, N., Bocchiola, D., Martin, M., Confortola, G., Salerno, F., Godone, D., D’Amico,
717 M. E., and Freppaz, M.: High export of nitrogen and dissolved organic carbon from an Alpine
718 glacier (Indren Glacier, NW Italian Alps), *Aquat. Sci.*, 81, 1–13,
719 <https://doi.org/10.1007/s00027-019-0670-z>, 2019.

720 Crawford, J. T., Dornblaser, M. M., Stanley, E. H., Clow, D. W., and Striegl, R. G.: Source
721 limitation of carbon gas emissions in high-elevation mountain streams and lakes, *J. Geophys.*
722 *Res. Biogeosciences*, 120, 952–964, <https://doi.org/10.1002/2014JG002861>, 2015.

723 Crawford, J. T., Hinckley, E. L. S., Litaor, M. I., Brahney, J., and Neff, J. C.: Evidence for
724 accelerated weathering and sulfate export in high alpine environments, *Environ. Res. Lett.*,
725 14, 124092, <https://doi.org/10.1088/1748-9326/ab5d9c>, 2019.

726 Deluigi, N., Lambiel, C., and Kanevski, M.: Data-driven mapping of the potential mountain
727 permafrost distribution, *Sci. Total Environ.*, 590–591, 370–380,
728 <https://doi.org/10.1016/j.scitotenv.2017.02.041>, 2017.

729 Donnini, M., Frondini, F., Probst, J. L., Probst, A., Cardellini, C., Marchesini, I., and
730 Guzzetti, F.: Chemical weathering and consumption of atmospheric carbon dioxide in the
731 Alpine region, *Glob. Planet. Change*, 136, 65–81,
732 <https://doi.org/10.1016/j.gloplacha.2015.10.017>, 2016.

733 Duarte, C. M. and Prairie, Y. T.: Prevalence of heterotrophy and atmospheric CO₂ emissions
734 from aquatic ecosystems, *Ecosystems*, 8, 862–870, [https://doi.org/10.1007/s10021-005-0177-](https://doi.org/10.1007/s10021-005-0177-4)
735 4, 2005.

736 Dümig, A., Smittenberg, R., and Kögel-knabner, I.: Concurrent evolution of organic and
737 mineral components during initial soil development after retreat of the Damma glacier ,
738 Switzerland, *Geoderma*, 163, 83–94, <https://doi.org/10.1016/j.geoderma.2011.04.006>, 2011.

739 Egli, M., Mavris, C., Mirabella, A., and Giaccai, D.: Soil organic matter formation along a

740 chronosequence in the Morteratsch proglacial area (Upper Engadine, Switzerland), *Catena*,
741 82, 61–69, <https://doi.org/10.1016/j.catena.2010.05.001>, 2010.

742 Eriksson, L., Johansson, E., Kettaneh-Wold, N., and Wold, S.: Multi-and megavariate data
743 analysis: Principles and applications., Umetrics AB, Umeå, Sweden, 2001.

744 Fasching, C., Ulseth, A. J., Schelker, J., Steniczka, G., and Battin, T. J.: Hydrology controls
745 dissolved organic matter export and composition in an Alpine stream and its hyporheic zone,
746 *Limnol. Oceanogr.*, 61, 558–571, <https://doi.org/10.1002/lno.10232>, 2016.

747 Fellman, J. B., Spencer, R. G. M., Hernes, P. J., Edwards, R. T., D'Amore, D. V., and Hood,
748 E.: The impact of glacier runoff on the biodegradability and biochemical composition of
749 terrigenous dissolved organic matter in near-shore marine ecosystems, *Mar. Chem.*, 121, 112–
750 122, <https://doi.org/10.1016/j.marchem.2010.03.009>, 2010.

751 Finstad, A. G., Andersen, T., Larsen, S., Tominaga, K., and Blumentrath, S.: From greening
752 to browning: Catchment vegetation development and reduced S-deposition promote organic
753 carbon load on decadal time scales in Nordic lakes, *Sci. Rep.*, 6, 31944,
754 <https://doi.org/10.1038/srep31944>, 2016.

755 Garcia, R. D., Reissig, M., Queimaliños, C. P., Garcia, P. E., and Dieguez, M. C.: Climate-
756 driven terrestrial inputs in ultraoligotrophic mountain streams of Andean Patagonia revealed
757 through chromophoric and fluorescent dissolved organic matter, *Sci. Total Environ.*, 521–522,
758 280–292, <https://doi.org/10.1016/j.scitotenv.2015.03.102>, 2015.

759 Gómez-Gener, L., Hotchkiss, E. R., Laudon, H., and Sponseller, R. A.: Integrating discharge-
760 concentration dynamics across carbon forms in a boreal landscape, *Water Resour. Res.*, 57, 1–
761 18, <https://doi.org/10.1029/2020WR028806>, 2021.

762 Gordon, N. D., McMahon, T. A., Finlayson, B. L., Gippel, C. J., and Nathan, R. J.: Stream
763 hydrology: an introduction for ecologists, John Wiley and Sons, 2004.

764 Guelland, K., Hagedorn, F., Smittenberg, R. H., Goransson, H., Bernasconi, S. M., Hajdas, I.,
765 and Kretzschmar, R.: Evolution of carbon fluxes during initial soil formation along the
766 forefield of Damma glacier, Switzerland, *Biogeochemistry*, 113, 545–561,
767 <https://doi.org/10.1007/s10533-012-9785-1>, 2013.

768 Guillemette, F. and del Giorgio, P. A.: Simultaneous consumption and production of
769 fluorescent dissolved organic matter by lake bacterioplankton, *Environ. Microbiol.*, 14, 1432–
770 1443, <https://doi.org/10.1111/j.1462-2920.2012.02728.x>, 2012.

771 Hagedorn, F., Gavazov, K., and Alexander, J. M.: Above- and belowground linkages shape
772 responses of mountain vegetation to climate change, *Science*, 365, 1119–1123,
773 <https://doi.org/10.1126/science.aax4737>, 2019.

774 Hall, R. O., Tank, J. L., Baker, M. A., Rosi-Marshall, E. J., and Hotchkiss, E. R.: Metabolism,
775 gas exchange, and carbon spiraling in rivers, *Ecosystems*, 19, 73–86,
776 <https://doi.org/10.1007/s10021-015-9918-1>, 2016.

777 Henne, P. D., Elkin, C. M., Reineking, B., Bugmann, H., and Tinner, W.: Did soil
778 development limit spruce (*Picea abies*) expansion in the Central Alps during the Holocene?
779 Testing a palaeobotanical hypothesis with a dynamic landscape model, *J. Bio.*, 38, 933–949,
780 <https://doi.org/10.1111/j.1365-2699.2010.02460.x>, 2011.

781 Hilton, R. G. and West, A. J.: Mountains, erosion and the carbon cycle, *Nat. Rev. Earth*
782 *Environ.*, 1, 284–299, <https://doi.org/10.1038/s43017-020-0058-6>, 2020.

783 Hodson, A., Tranter, M., and Vatne, G.: Contemporary rates of chemical denudation and
784 atmospheric CO₂ sequestration in glacier basins: an Arctic perspective, *Earth Surf. Process.*
785 *Landforms*, 25, 1447–1471, [https://doi.org/10.1002/1096-9837\(200012\)25:13<1447::AID-ESP156>3.0.CO;2-9](https://doi.org/10.1002/1096-9837(200012)25:13<1447::AID-ESP156>3.0.CO;2-9), 2000.

787 Hoffmann, U., Hoffmann, T., Jurasinski, G., Glatzel, S., and Kuhn, N. J.: Assessing the
788 spatial variability of soil organic carbon stocks in an alpine setting (Grindelwald, Swiss Alps),
789 *Geoderma*, 232–234, 270–283, <https://doi.org/10.1016/j.geoderma.2014.04.038>, 2014.

790 Hongve, D., Riise, G., and Kristiansen, J. F.: Increased colour and organic acid concentrations
791 in Norwegian forest lakes and drinking water – a result of increased precipitation?, *Aquat.*
792 *Sci.*, 66, 231–238, <https://doi.org/10.1007/s00027-004-0708-7>, 2004.

793 Hood, E., Fellman, J., Spencer, R. G. M., Hernes, P. J., Edwards, R., Damore, D., and Scott,
794 D.: Glaciers as a source of ancient and labile organic matter to the marine environment,
795 *Nature*, 462, 1044–1047, <https://doi.org/10.1038/nature08580>, 2009.

796 Horgby, Å., Gómez-Gener, L., Escoffier, N., and Battin, T. J.: Dynamics and potential drivers
797 of CO₂ concentration and evasion across temporal scales in high-alpine streams, *Environ. Res.*
798 *Let.*, 14, 124082, <https://doi.org/10.1088/1748-9326/ab5cb8>, 2019a.

799 Horgby, Å., Boix Canadell, M., Ulseth, A. J., Vennemann, T. W., and Battin, T. J.: High-
800 resolution spatial sampling identifies groundwater as driver of CO₂ dynamics in an alpine
801 stream network, *J. Geophys. Res. Biogeosciences*, 124, 1961–1976,
802 <https://doi.org/10.1029/2019JG005047>, 2019b.

803 Horgby, Å., Segatto, P. L., Bertuzzo, E., Lauerwald, R., Lehner, B., Ulseth, A. J.,
804 Vennemann, T. W., and Battin, T. J.: Unexpected large evasion fluxes of carbon dioxide from
805 turbulent streams draining the world’s mountains, *Nat. Commun.*, 10, 4888,
806 <https://doi.org/10.1038/s41467-019-12905-z>, 2019c.

807 Hotchkiss, E. R., Hall Jr, R. O., Sponseller, R. A., Butman, D., Klaminder, J., Laudon, H.,
808 Rosvall, M., and Karlsson, J.: Sources of and processes controlling CO₂ emissions change
809 with the size of streams and rivers, *Nat. Geosci.*, 8, 696–699,
810 <https://doi.org/10.1038/ngeo2507>, 2015.

811 Imbeau, E. and Vincent, W. F.: Hidden stores of organic matter in northern lake ice: selective
812 retention of terrestrial particles, phytoplankton and labile carbon, *J. Geophys. Res.*
813 *Biogeosciences*, 126, e2020JG006233, <https://doi.org/10.1029/2020JG006233>, 2021.

814 Kida, M., Kojima, T., Tanabe, Y., Hayashi, K., Kudoh, S., Maie, N., and Fujitake, N.: Origin,
815 distributions, and environmental significance of ubiquitous humic-like fluorophores in
816 Antarctic lakes and streams, *Water Res.*, 163, 114901,
817 <https://doi.org/10.1016/j.watres.2019.114901>, 2019.

818 Kida, M., Fujitake, N., Kojima, T., Tanabe, Y., Hayashi, K., Kudoh, S., and Dittmar, T.:
819 Dissolved organic matter processing in pristine Antarctic streams, *Environ. Sci. Technol.*, 55,
820 10175–10185, <https://doi.org/10.1021/acs.est.1c03163>, 2021.

821 Klaar, M. J., Kidd, C., Malone, E., Bartlett, R., Pinay, G., Chapin, F. S., and Milner, A.:
822 Vegetation succession in deglaciated landscapes : implications for sediment and landscape
823 stability, *Earth Surf. Process. Landforms*, 40, 1088–1100, <https://doi.org/10.1002/esp.3691>,
824 2014.

825 Kneib, M., Cauvy-Fraunié, S., Escoffier, N., Boix Canadell, M., Horgby, and Battin, T. J.:

826 Glacier retreat changes diurnal variation intensity and frequency of hydrologic variables in
827 Alpine and Andean streams, *J. Hydrol.*, 583, 124578,
828 <https://doi.org/10.1016/j.jhydrol.2020.124578>, 2020.

829 Knight, J. and Harrison, S.: Mountain glacial and paraglacial environments under global
830 climate change: Lessons from the past, future directions and policy implications, *Geogr. Ann.*
831 *Ser. A Phys. Geogr.*, 96, 245–264, <https://doi.org/10.1111/geoa.12051>, 2014.

832 Kritzberg, E. S., Hasselquist, E. M., Martin, S., Olsson, O., Stadmark, J., and Valinia, S.:
833 Browning of freshwaters: Consequences to ecosystem services, underlying drivers, and
834 potential mitigation measures, *Ambio*, 49, 375–390, <https://doi.org/10.1007/s13280-019-01227-5>, 2019.

836 Lafrenière, M. J. and Sharp, M. J.: The concentration and fluorescence of dissolved organic
837 carbon (DOC) in glacial and nonglacial catchments: interpreting hydrological flow routing
838 and DOC sources, *Arctic, Antarct. Alp. Res.*, 36, 156–165, [https://doi.org/10.1657/1523-0430\(2004\)036\[0156:TCAFOD\]2.0.CO;2](https://doi.org/10.1657/1523-0430(2004)036[0156:TCAFOD]2.0.CO;2), 2004.

840 Mackay, J. D., Barrand, N. E., Hannah, D. M., Krause, S., Jackson, C. R., Everest, J.,
841 Aoalgeirsdóttir, G., and Black, A.: Future evolution and uncertainty of river flow regime
842 change in a deglaciating river basin, *Hydrol. Earth Syst. Sci.*, 23, 1833–1865,
843 <https://doi.org/10.5194/hess-23-1833-2019>, 2019.

844 Marx, A., Dusek, J., Jankovec, J., Sanda, M., Vogel, T., van Geldern, R., Hartmann, J., and
845 Barth, J. A. C.: A review of CO₂ and associated carbon dynamics in headwater streams: A
846 global perspective, *Rev. Geophys.*, 55, 560–585, <https://doi.org/10.1002/2016RG000547>,
847 2017.

848 Marzolf, N. S., Small, G. E., Oviedo-Vargas, D., Ganong, C. N., Duff, J. H., Ramírez, A.,
849 Pringle, C. M., Genereux, D. P., and Ardón, M.: Partitioning inorganic carbon fluxes from
850 paired O₂-CO₂ gases in a headwater stream, Costa Rica, *Biogeochemistry*, 160, 259–273,
851 <https://doi.org/10.1007/s10533-022-00954-4>, 2022.

852 Massicotte, P.: eemR: tools for pre-processing emission-excitation-matrix (EEM)
853 fluorescence data, R Packag. version 1.0.1, 2019.

854 Masson-Delmotte, V., Zhai, P., Pirani, A., Connors, S. L., Péan, C., Berger, S., Caud, N.,
855 Chen, Y., Goldfarb, L., Gomis, M. I., Huang, M., Leitzell, K., Lonnoy, E., Matthews, J. B. R.,
856 Maycock, T. K., Waterfield, T., Yelekçi, O., Yu, R., and Zhou, B. (Eds.): Climate change
857 2021: The physical science basis. Working Group I contribution to the IPCC Sixth
858 Assessment Report, Cambridge University Press, Cambridge, United Kingdom and New
859 York, NY, USA, <https://doi.org/10.1017/9781009157896>, 2021.

860 Milner, A. M., Brown, L. E., and Hannah, D. M.: Hydroecological response of river systems
861 to shrinking glaciers, *Hydrol. Process.*, 23, 62–77, <https://doi.org/10.1002/hyp>, 2009.

862 Milner, A. M., Khamis, K., Battin, T. J., Brittain, J. E., Barrand, N. E., Füreder, L., Cauvy-
863 Fraunié, S., Gíslason, G. M., Jacobsen, D., Hannah, D. M., Hodson, A. J., Hood, E., Lencioni,
864 V., Ólafsson, J. S., Robinson, C. T., Tranter, M., and Brown, L. E.: Glacier shrinkage driving
865 global changes in downstream systems, *Proc. Natl. Acad. Sci. U. S. A.*, 114, 9770–9778,
866 <https://doi.org/10.1073/pnas.1619807114>, 2017.

867 Murphy, K. R., Butler, K. D., Spencer, R. G. M., Stedmon, C. A., Boehme, J. R., and Aiken,
868 G. R.: Measurement of dissolved organic matter fluorescence in aquatic environments: an
869 interlaboratory comparison, *Environ. Sci. Technol.*, 44, 9405–9412,

870 <https://doi.org/10.1021/es102362t>, 2010.

871 Murphy, K. R., Stedmon, C. A., Graeber, D., and Bro, R.: Fluorescence spectroscopy and
872 multi-way techniques. *PARAFAC, Anal. Methods*, 5, 6557,
873 <https://doi.org/10.1039/c3ay41160e>, 2013.

874 Murphy, K. R., Stedmon, C. A., Wenig, P., and Bro, R.: OpenFluor – an online spectral
875 library of auto- fluorescence by organic compounds in the environment †, *Anal. Methods*, 6,
876 658–661, <https://doi.org/10.1039/c3ay41935e>, 2014.

877 Nash, M. S. and Chaloud, D. J.: Partial least square analyses of landscape and surface water
878 biota associations in the Savannah River basin, *ISRN Ecol.*, 2011, 1–11,
879 <https://doi.org/10.5402/2011/571749>, 2011.

880 Onderka, M., Wrede, S., Rodný, M., Pfister, L., Hoffmann, L., and Krein, A.: Hydrogeologic
881 and landscape controls of dissolved inorganic nitrogen (DIN) and dissolved silica (DSi) fluxes
882 in heterogeneous catchments, *J. Hydrol.*, 450–451, 36–47,
883 <https://doi.org/10.1016/j.jhydrol.2012.05.035>, 2012.

884 Paillex, A., Siebers, A. R., Ebi, C., Mesman, J., and Robinson, C. T.: High stream
885 intermittency in an alpine fluvial network: Val Roseg, Switzerland, *Limnol. Oceanogr.*, 65,
886 557–568, <https://doi.org/10.1002/lno.11324>, 2020.

887 Pain, A. J., Martin, J. B., Martin, E. E., Rahman, S., and Ackermann, P.: Differences in the
888 quantity and quality of organic matter exported from Greenlandic glacial and deglaciated
889 watersheds, *Global Biogeochem. Cycles*, 34, 1–20, <https://doi.org/10.1029/2020GB006614>,
890 2020.

891 Pawellek, F. and Veizer, J.: Carbon cycle in the upper Danube and its tributaries: $\delta^{13}\text{C}$ -DIC
892 constraints, *Isr. J. Earth Sci.*, 43, 187–194, 1994.

893 St. Pierre, K. A., St. Louis, V. L., Schiff, S. L., Lehnher, I., Dainard, P. G., Gardner, A. S.,
894 Aukes, P. J. K., and Sharp, M. J.: Proglacial freshwaters are significant and previously
895 unrecognized sinks of atmospheric CO_2 , *Proc. Natl. Acad. Sci. U. S. A.*, 116, 17690–17695,
896 <https://doi.org/10.1073/pnas.1904241116>, 2019.

897 Plummer, L. N. and Busenberg, E.: The solubilities of calcite, aragonite and vaterite in CO_2 -
898 H_2O solutions between 0 and 90°C , and an evaluation of the aqueous model for the system
899 $\text{CaCO}_3\text{-CO}_2\text{-H}_2\text{O}$, *Geochim. Cosmochim. Acta*, 46, 1011–1040, [https://doi.org/10.1016/0016-7037\(82\)90056-4](https://doi.org/10.1016/0016-7037(82)90056-4), 1982.

901 Pucher, M., Wunsch, U., Weigelhofer, G., Murphy, K., Hein, T., and Graeber, D.: staRdom:
902 versatile software for analyzing spectroscopic data of dissolved organic matter in R, *Water*,
903 11, 2366, <https://doi.org/10.3390/w11112366>, 2019.

904 Rehn, L., Sponseller, R. A., Laudon, H., and Wallin, M. B.: Long-term changes in dissolved
905 inorganic carbon across boreal streams caused by altered hydrology, *Limnol. Oceanogr.*, 68,
906 409–423, <https://doi.org/10.1002/lno.12282>, 2022.

907 Roulet, N. and Moore, T. R.: Browning the waters, *Nature*, 444, 283–284,
908 <https://doi.org/10.1038/444283a>, 2006.

909 Rumpf, S. B., Gravey, M., Brönnimann, O., Luoto, M., Cianfrani, C., Mariethoz, G., and
910 Guisan, A.: From white to green: Snow cover loss and increased vegetation productivity in
911 the European Alps, *Science*, 376, 1119–1122, 2022.

- 912 Sharp, M., Tranter, M., Brown, G. H., and Skidmore, M.: Rates of chemical denudation and
 913 CO₂ drawdown in a glacier-covered alpine catchment, *Geology*, 23, 61–64,
 914 [https://doi.org/10.1130/0091-7613\(1995\)023<0061:ROCDAC>2.3.CO;2](https://doi.org/10.1130/0091-7613(1995)023<0061:ROCDAC>2.3.CO;2), 1995.
- 915 Singer, G. A., Fasching, C., Wilhelm, L., Niggemann, J., Steier, P., Dittmar, T., and Battin, T.
 916 J.: Biogeochemically diverse organic matter in Alpine glaciers and its downstream fate, *Nat.*
 917 *Geosci.*, 5, 710–714, <https://doi.org/10.1038/ngeo1581>, 2012.
- 918 Skidmore, M., Sharp, M., and Tranter, M.: Kinetic isotopic fractionation during carbonate
 919 dissolution in laboratory experiments : implications for detection of microbial CO₂ signatures
 920 using $\delta^{13}\text{C}$ -DIC, *Geochim. Cosmochim. Acta*, 68, 4309–4317,
 921 <https://doi.org/10.1016/j.gca.2003.09.024>, 2004.
- 922 Spencer, R. G. M., Vermilyea, A., Fellman, J., Raymond, P., Stubbins, A., Scott, D., and
 923 Hood, E.: Seasonal variability of organic matter composition in an Alaskan glacier out flow:
 924 insights into glacier carbon sources, *Environ. Res. Lett.*, 9, 055005,
 925 <https://doi.org/10.1088/1748-9326/9/5/055005>, 2014.
- 926 Stedmon, C. A. and Bro, R.: Characterizing dissolved organic matter fluorescence with
 927 parallel factor analysis: a tutorial, *Limnol. Oceanogr. Fluids Environ.*, 6, 572–579,
 928 <https://doi.org/10.4319/lom.2008.6.572>, 2008.
- 929 Torres, M. A., Moosdorf, N., Hartmann, J., Adkins, J. F., and West, A. J.: Glacial weathering,
 930 sulfide oxidation, and global carbon cycle feedbacks, *Proc. Natl. Acad. Sci. U. S. A.*, 114,
 931 8716–8721, <https://doi.org/10.1073/pnas.1702953114>, 2017.
- 932 Tranter, M.: Geochemical weathering in glacial and proglacial environments, *Treatise on*
 933 *Geochemistry*, 5, 605, <https://doi.org/10.1016/B0-08-043751-6/05078-7>, 2003.
- 934 Ulseth, A. J., Hall, R. O., Boix Canadell, M., Madinger, H. L., Niayifar, A., and Battin, T. J.:
 935 Distinct air–water gas exchange regimes in low- and high-energy streams, *Nat. Geosci.*, 12,
 936 259–263, <https://doi.org/10.1038/s41561-019-0324-8>, 2019.
- 937 Wallin, M. B., Grabs, T., Buffam, I., Laudon, H., Ågren, A., Öquist, M. G., and Bishop, K.:
 938 Evasion of CO₂ from streams - The dominant component of the carbon export through the
 939 aquatic conduit in a boreal landscape, *Glob. Chang. Biol.*, 19, 785–797,
 940 <https://doi.org/10.1111/gcb.12083>, 2013.
- 941 Wanninkhof, R.: Relationship between wind speed and gas exchange over the ocean revisited,
 942 *Limnol. Oceanogr. Methods*, 12, 351–362, <https://doi.org/10.4319/lom.2014.12.351>, 2014.
- 943 Wietrzyk-Pełka, P., Rola, K., Szymański, W., and Węgrzyn, M. H.: Organic carbon
 944 accumulation in the glacier forelands with regard to variability of environmental conditions in
 945 different ecogenesis stages of High Arctic ecosystems, *Sci. Total Environ.*, 717, 1–12,
 946 <https://doi.org/10.1016/j.scitotenv.2019.135151>, 2020.
- 947 Wold, S., Ruhe, A., Wold, H., and Dunn III, W. J.: The collinearity problem in linear
 948 regression. The partial least squares (PLS) approach to generalized inverses, *SIAM J. Sci.*
 949 *Stat. Comput.*, 5, 735–743, 1984.
- 950 Zah, R. and Uehlinger, U.: Particulate organic matter inputs to a glacial stream ecosystem in
 951 the Swiss Alps, *Freshw. Biol.*, 46, 1597–1608, <https://doi.org/10.1046/j.1365-2427.2001.00847.x>, 2001.
- 953 Zhou, Y., Zhou, L., He, X., Jang, K. S., Yao, X., Hu, Y., Zhang, Y., Li, X., Spencer, R. G. M.,
 954 Brookes, J. D., and Jeppesen, E.: Variability in dissolved organic matter composition and

955 biolability across gradients of glacial coverage and distance from glacial terminus on the
956 Tibetan Plateau, *Environ. Sci. Technol.*, 53, 12207–12217,
957 <https://doi.org/10.1021/acs.est.9b03348>, 2019.

958

959 Table 1: Catchment characteristics.

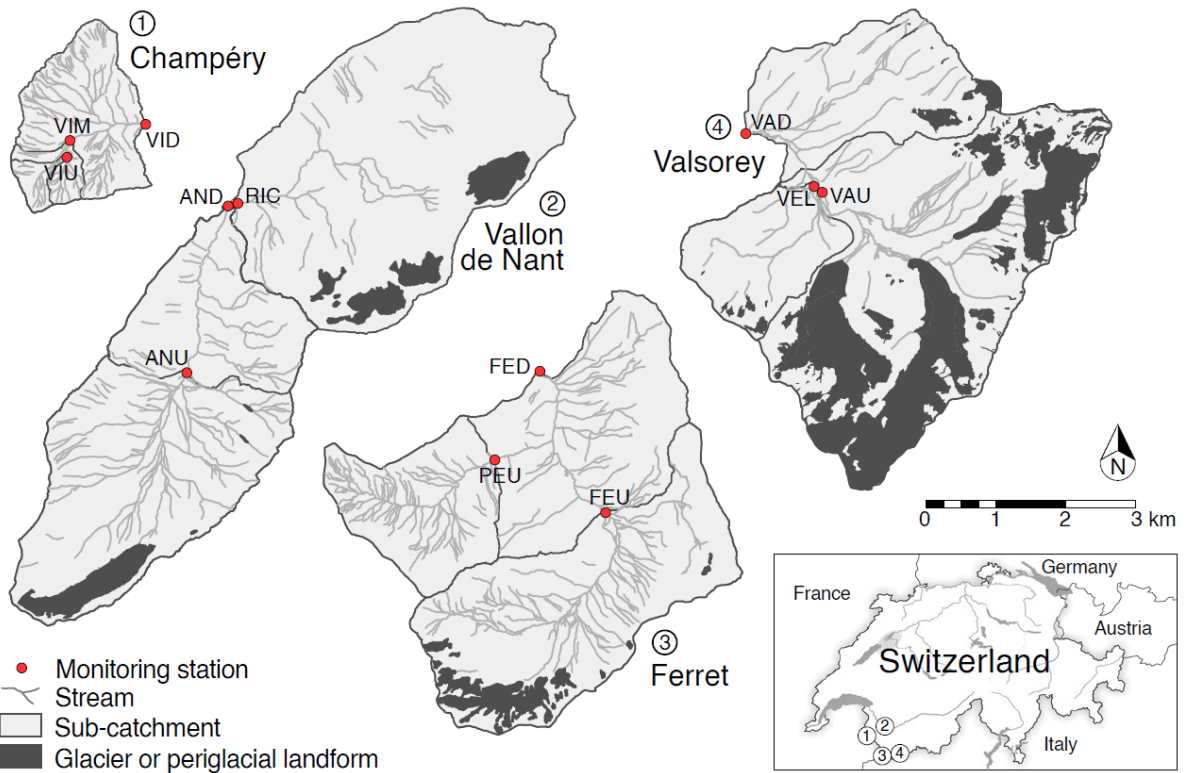
Catchment	ID	Station	Station altitude (m a.s.l.)	Area (km ²)	Glacier coverage (%)	Vegetation coverage (%)	Dominant lithology
Valsorey	VAD	Down	1936	23.2	27.4	24.2	Blue-grey schists, gneiss, schist
	VAU	Up	2148	18.1	33.5	21.1	
	VEL	Tributary	2161	3.11	0	56.7	
Val Ferret	FED	Down	1773	20.2	3.41	62.4	Limestone, sandstone, schist
	FEU	Up	1996	9.33	7.40	46.3	
	PEU	Tributary	2024	3.97	0	70.2	
Vallon de Nant	AND	Down	1197	13.4	4.58	63.9	Limestone; calcareous shale; flysch
	AVU	Up	1465	8.99	6.80	54.0	
	RIC	Tributary	1192	14.3	6.38	64.2	
Champéry	VID	Down	1416	3.64	0	94.0	Flysch, limestone; shale
	VIM	Middle	1630	0.74	0	86.1	
	VIU	Up	1689	0.31	0	80.9	

960

961 Table 2: Median concentration of DOC and DIC, percent saturation of CO₂ and O₂, and
 962 isotopic composition of DIC for the 12 sites. Concentration and isotopic composition are
 963 summarized from grab samples, while CO₂ and O₂ saturation are summarized from sensor
 964 data.

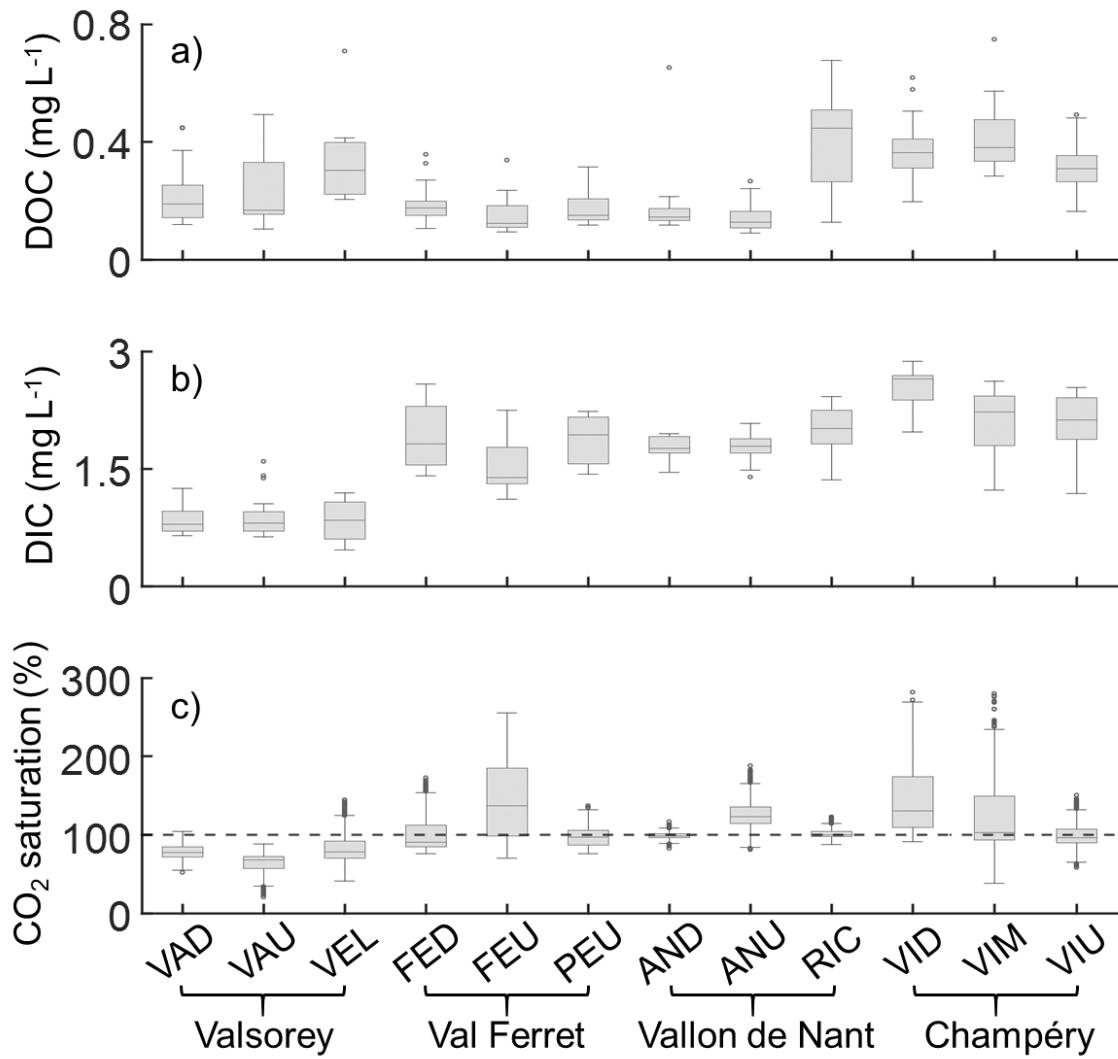
Catchment	Station	DOC (mg L ⁻¹)	DIC (mg L ⁻¹)	CO _{2,sat} (%)	O _{2,sat} (%)	δ ¹³ C-DIC (‰)
Valsorey	Down	0.19	0.79	77.4	98.6	-5.34
	Up	0.17	0.80	68,1	99.0	-6.08
	Tributary	0.30	0.84	77.7	98.3	-6.57
Val Ferret	Down	0.18	1.82	90.7	99.3	-4.04
	Up	0.12	1.38	137	99.0	-3.98
	Tributary	0.15	1.93	97.0	99.5	-3.67
Vallon de Nant	Down	0.14	1.76	98.4	99.8	-5.10
	Up	0.13	1.79	123	99.0	-6.31
	Tributary	0.45	2.01	100	99.2	-6.96
Champery	Down	0.36	2.65	130	99.2	-8.45
	Middle	0.38	2.22	103	99.5	-9.29
	Up	0.31	2.13	96.2	98.8	-9.76

965



967
968
969

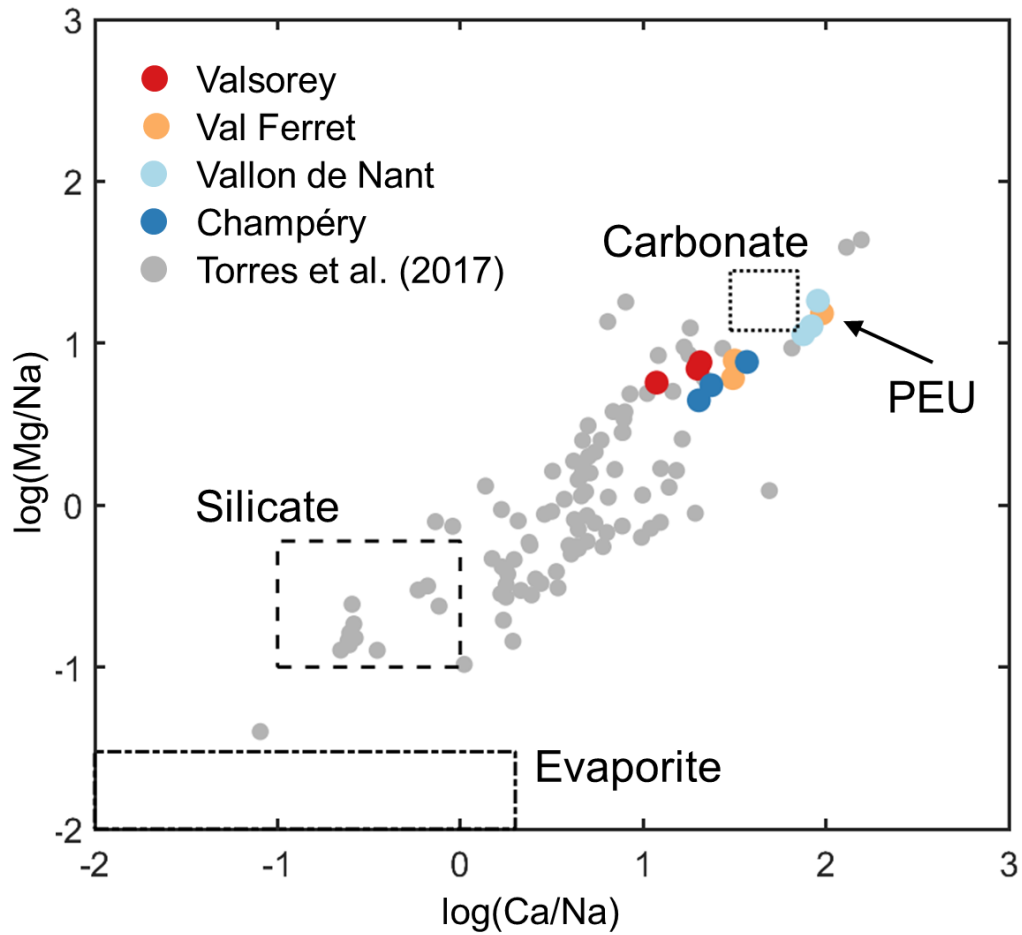
Figure 1: Map of the 12 study sites within four catchments of the Alps in southwestern Switzerland (glacial cover and stream network from swissTLM3D; swisstopo).



970

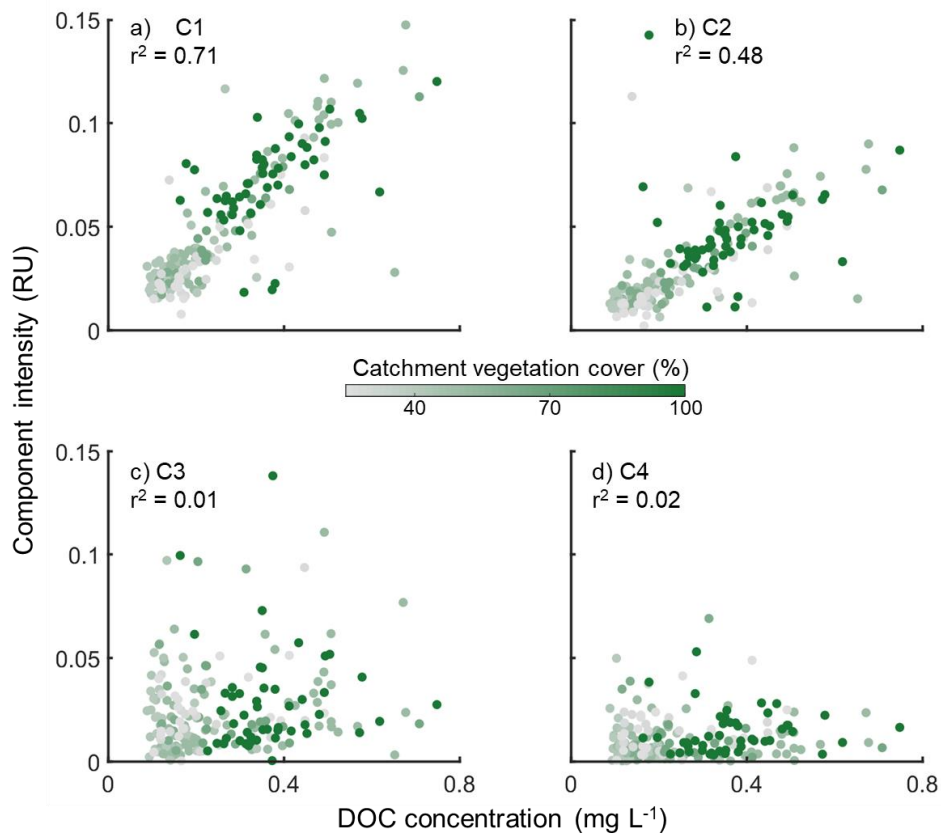
971 Figure 2: Boxplots of a) DOC and b) DIC concentration (mg L⁻¹) from grab samples, and c)

972 CO₂ saturation (%) derived from sensor measurements.



973
 974 Figure 3: Stoichiometry of dissolved ion in the twelve study streams and from a global
 975 database of 95 glacier-fed streams (Torres et al., 2017). The range of each lithological end-
 976 member are shown by the boxes. The tributary stream in the Val Ferret catchment (PEU) is
 977 shown as it is clearly distinguished from the main stream locations.

978



979

980

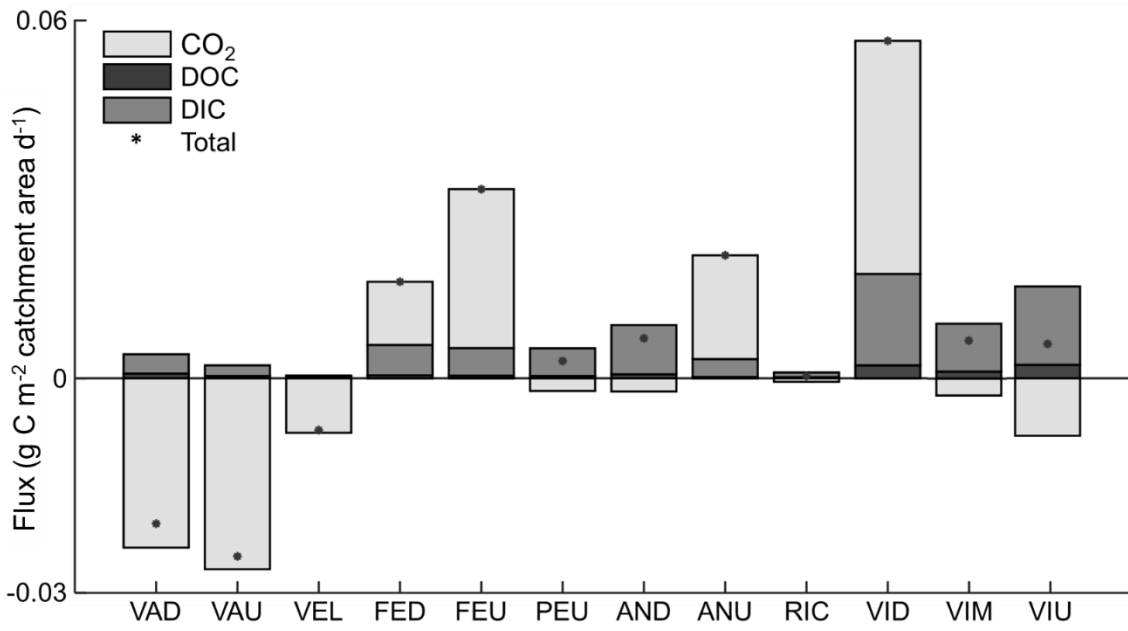
981

982

983

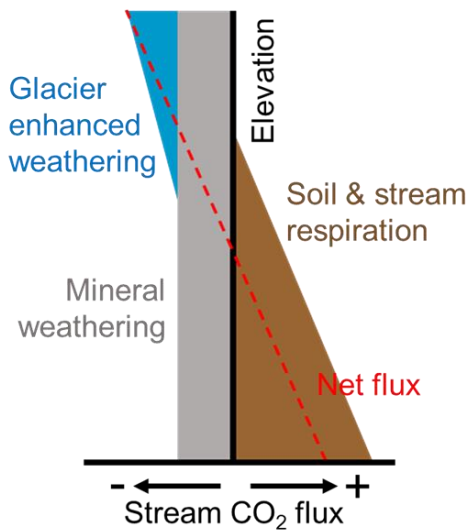
984

Figure 4: Intensity of the four components within the PARAFAC model against DOC concentration from grab samples, with catchment vegetation cover shown by color. a) Component 1 and b) component 2 represent humic-like compounds while c) component 3 and d) component 4 represent proteinaceous compounds. The coefficient of determination (r^2) is shown for each linear regression.



985
 986
 987
 988

Figure 5: Estimated annual fluxes of the dissolved carbon components (CO₂, DOC, and DIC) normalized for catchment area. DOC and DIC are downstream fluxes, while CO₂ is a vertical flux. The DIC flux includes downstream transport of CO₂.



989
 990 Figure 6: Conceptual model of processes affecting CO₂ saturation, and thus direction of flux,
 991 across glacier, soil, and elevation gradients within glacierized catchments. Geochemical
 992 weathering is important across the entire landscape, but is enhanced under glaciated
 993 conditions and nearness to the glacier. As vegetation and soil develop at lower elevation,
 994 terrestrial inputs add CO₂ through direct inputs from soil respiration and from organic carbon
 995 inputs which fuel in-stream respiration. The net balance of these processes determines the
 996 CO₂ saturation. In the aerial image of the Valsorey catchment, the transition from glacier to
 997 vegetation cover can be seen directly (from Google Earth 2023).